



Synthesis and characterization of ZnO nanoparticles via zeolitic imidazolate framework-8 and its application for removal of dyes

N. Hassan ^a, A. Shahat ^b, A. El-Didamony ^c, M.G. El-Desouky ^a, A.A. El-Binary ^{d,*}

^a Chemistry Department, Faculty of Science, Port Said University, Port Said, 42511, Egypt

^b Chemistry Department, Faculty of Science, Suez University, Suez, 43518, Egypt

^c Chemistry Department, Faculty of Science, Zagazig University, Zagazig, 44519, Egypt

^d Chemistry Department, Faculty of Science, Damietta University, Damietta, 34517, Egypt

ARTICLE INFO

Article history:

Received 26 November 2019

Received in revised form

4 March 2020

Accepted 5 March 2020

Available online 10 March 2020

Keywords:

ZnO nanoparticles

Adsorption

Kinetics

Isotherm

Thermodynamics

ABSTRACT

Zinc oxide (ZnO) nanoparticles were obtained via calcination of zeolitic imidazolate framework-8 (ZIF-8). The activities of prepared ZnO nanoparticles at different temperature 450, 550, and 650 °C were investigated for the adsorption of acid red 57 (AR57) and remazole red (RR) dye. The synthesized ZnO nanoparticles were characterized by different spectroscopic studies such as FTIR, X-ray diffraction, energy-dispersive X-ray spectroscopy, N₂ adsorption-desorption and pH titration for determination of Zero-point charge (pH_{ZPC}). The mechanism of adsorption behavior of AR57 and RR are studied with respect to temperature, pH and concentration. Experimental data indicated that the adsorption capacity of ZnO for AR57 and RR was higher in acidic rather than in basic solutions. The activation energy of adsorption was also evaluated for the adsorption of AR57 and RR onto ZnO nanoparticles. Langmuir and Freundlich adsorption models were also applied to describe the equilibrium isotherms and the isotherm constants. The pseudo-first-order and pseudo-second-order model equations were used to analyze the kinetics of the adsorption process. The adsorption efficiency of ZnO nanoparticles was found in the order: 450 > 550 > 650 °C. The activation energy, enthalpy, change of free energy and entropy of adsorption were also evaluated for the adsorption of AR57 and RR onto ZnO nanoparticles. The thermodynamics of the adsorption indicated spontaneous and exothermic nature of the process.

© 2020 Elsevier B.V. All rights reserved.

1. Introduction

Dyes have been used for coloring industrial products such as textile, food, plastics, paper, tannery and cosmetics [1]. Dyes can be classified as cationic dye (basic dyes), anionic dye (acid dyes) and non-ionic (dispersed dyes) [2]. The treatment of industrial waste water to remove color from it has become environmentally important [3]. The anionic dyes in aqueous solution carry a net negative charge due to the sulphonate groups, while the cationic dyes carry a net positive charge due to the protonated amine or sulphur containing groups [4]. Thus, it is imperative to treat these effluent dyes before releasing into the aqueous environment. Also, they have aromatic structure which makes them more stable and difficult to biodegrade [4]. The methods were used for removing color effluents from water include oxidation [5], electro-chemical

[6], coagulation [7], solvent extraction [8], photocatalytic degradation [9], ozonation [10], adsorption [11], etc. but, the adsorption technique is considered to be favorable than other techniques. Because, it's ease of operation, high efficiency, simple design and the important point its low cost [12].

Zinc oxide has unique properties that have been utilized in many types of applications, and the surface properties of this material have been investigated by various approaches. ZnO is one of the most commonly used materials for adsorption applications owing to its high chemical stability, low cost, low toxicity, and excellent oxidation properties. These parameters depend on the method of preparation of ZnO, which can be formed in several morphologies and sizes, especially in nanoscale dimensions [13].

In this work, the BET surface area for ZnO was 37.674 m²/g and the total pore volume taken at a saturation pressure and expressed as liquid volume is 0.1178 cm³/g and average pore diameter 12.5068 nm. The BJH surface area was 51.139 m²/g and pore volume 0.125 cm³/g. SEM analysis approved that ZnO was nanoparticles as its average diameter was ~38.84 nm. The observed diffraction peaks

* Corresponding author.

E-mail address: abinary@yahoo.com (A.A. El-Binary).

connected with well crystallized ZnO indicate the formation of the hexagonal wurtzite structure. The energy dispersive X-ray analysis was performed to know the elemental composition of zinc and oxygen present in the ZnO nanoparticles. The thermodynamic parameters such as ΔG , ΔS and ΔH were calculated from the intercepts and slopes of the linear variation of $\ln K$ vs. $1/T$. The adsorption equilibrium showed that the Langmuir equation represented best fit of the experimental data than others for both AR57 and RR dye. The adsorption kinetics was found to follow pseudo-second-order kinetic model, suggesting a chemisorption process. Adsorption thermodynamic study suggested that the adsorption reactions were spontaneous, endothermic and thermodynamically favorable.

2. Materials and methods

2.1. Chemicals

Chemicals were used as received without any further purification process. They include zinc nitrate hexahydrate (99%, Tianjin Kemiou Chemical Reagent, China), 2-methylimidazole (Hmim) (Sinopharm chemical reagent Co. Ltd., China), ammonium hydroxide solution (NH_3 , 25–28%, Nanjing Chemical Reagent Co. Ltd., China), anhydrous ethanol (99.7%, Sinopharm chemical reagent Co. Ltd., China). Acid Red 57 and Remazol Red were purchased from Merck KGaA, 64,271 Darmstadt, Germany.

2.2. Preparation of the adsorbent

ZIF-8 was synthesized according to previously reported studies [14]. In a typical synthesis, 2.97 g of zinc nitrate hexahydrate ($\text{Zn}(\text{NO}_3)_2 \cdot 6\text{H}_2\text{O}$) was dissolved in 3 g of deionized water; 1.64 g of Hmim was added in 20.75 mL ammonium hydroxide solution; after that zinc nitrate and Hmim solutions were mixed together. The solution immediately turned into milk-like suspension, and stirred for 10 min at room temperature to complete the crystallization. The sample was collected by centrifugation and washed with deionized water three times until the final product had pH value of 7, then dried at 60 °C overnight. ZnO was obtained via calcination ZIF-8 at 450, 550 and 650 °C for 2 h with heating rate of 5 °C.min⁻¹.

2.3. Preparation of adsorbate

Stock solutions of AR57 and RR (1×10^{-3} M) were prepared by dissolving an accurate quantity of AR57 and RR individual (Tables 1 and 2). Deionized water was used in preparing the stock solutions and also throughout the experimental analysis.

2.4. Characterization of ZnO nanoparticles

FTIR analysis was carried out using a JASCO-FT/IR-4100 spectrometer (Jasco, Easton, MD, USA): the finely grinded sample of ZnO was included into KBr discs prior to analysis in the wavenumber range 400–4000 cm⁻¹. Structural deviations of the as-prepared ZnO samples was investigated by X-ray diffraction (XRD) system by a Shimadzu XRD-6000 diffract meter (Shimadzu Corporation, Tokyo, Japan) equipped with Cu K α radiation ($\lambda = 1.54 \text{ \AA}$). The 2 θ range was varied between 5 and 80° at a scanning rate of 0.02°. The crystal system, space group and lattice parameters values were measured and optimized using CRYSFIRE and CHEKCELL computer databases [15]. UV–visible spectrophotometer (HACH LANGE DR5000) was working for absorbance measurements of samples using 1.0 cm quartz cell. N₂ sorption isotherms were recorded at the boiling temperature of liquid nitrogen (–196 °C) on ASAP 2020 (Micrometrics, USA). Before analysis, the particles were exposed to

vacuum (5×10^{-3} torr) at 200 °C in order to ensure a clean surface. Using Brunauer-Emmett-Teller (BET) method, from which the Brunauer-Emmett-Teller (BET) surface area and Barrett-Joyner-Halenda (BJH) pore volume were calculated. The surface morphology of ZnO was studied using scanning electron microscope (SEM) investigation at accelerating voltages of 20 kV (JEOL-JSM-6510 LV) using gold coating examination. The elemental distribution of ZnO was examined using the energy-dispersive X-ray spectroscopy (EDX) and taken on a Leo1430VP microscope with operating voltage 5 kV. HANNA instrument pH meter (model 211) was used for pH modification.

2.5. Experimental design for batch adsorption studies

Batch adsorption techniques were performed to study the effect of parameters such as adsorbent dose, contact time, initial concentration, solution pH and temperature for the removal of AR57 and RR on ZnO nanoparticles. The process was carried out by shaking 50 mL conical flasks containing 0.02 g of ZnO and 25 mL of dye solutions of desired concentration with adjusted pH using a shaker water bath at a constant speed of 200 rpm. To observe the effect of adsorbent dose on dyes adsorption, different amounts of ZnO (varying from 0.01 to 0.10 g) were respectively added into initial concentration of AR57 (1.22×10^{-3} M) and RR (1.06×10^{-3} M) solution at 25 °C and the desired pH until the equilibrium time was reached. The effect of pH on AR57 and RR adsorption was studied by varying the pH from 2 to 12 and adjusted to the desired value using 0.1 mol/L HCl and 0.1 mol/L NaOH solutions. At the end of the adsorption period, the supernatant solution was separated from the adsorbent by centrifuge at 3000 rpm for 5 min. Then the concentration of the residual dye was determined spectrophotometrically by monitoring the absorbance at 512 nm for AR57 and 541 nm for RR using UV–Vis spectrophotometer. Percentage of dye removal (R) was calculated using Eq. (1):

$$R = 100(C_0 - C_t) / C_0 \quad (1)$$

where C_0 (mmolg⁻¹) and C_t (mmolg⁻¹) are dye concentration initially and at time t, respectively.

For adsorption process, dye solutions of different concentrations (8.85×10^{-4} – 3.63×10^{-3} M) for AR57 and (3.7×10^{-5} – 1.06×10^{-3} M) for RR was agitated with 0.02 g of adsorbent until the equilibrium was achieved. Equilibrium adsorption capacity, q_e (mmol dye per g adsorbent) was calculated from the following Eq. (2):

$$q_e = V(C_0 - C_t) / W \quad (2)$$

where C_t (mmolg⁻¹) is the dye concentration at equilibrium, V (L) is the volume of solution and W (g) is the weight of adsorbent.

The procedures of kinetic experiment were identical with those of equilibrium tests. At predetermined moments, aqueous samples (5 mL) were taken from the solution, the liquid was separated from the adsorbent by centrifuge and concentration of dye in solution was determined spectrophotometrically. The amount of dye adsorbed at time t, q_t (mmolg⁻¹) was calculated by following Eq. (3):

$$q_t = V(C_0 - C_t) / m \quad (3)$$

where C_0 (ppm) is the initial dye concentration, C_t (ppm) the dye concentration at any time t, V (L) the volume of the solution and m (g) is the mass of the adsorbent.

The adsorption isotherms which indicate that the AR57 and RR adsorption behavior was investigated at 20, 25, 30, 35, 40 and 45 °C

Table 1
Properties of the adsorbate (Acid Red 57) used in the study.

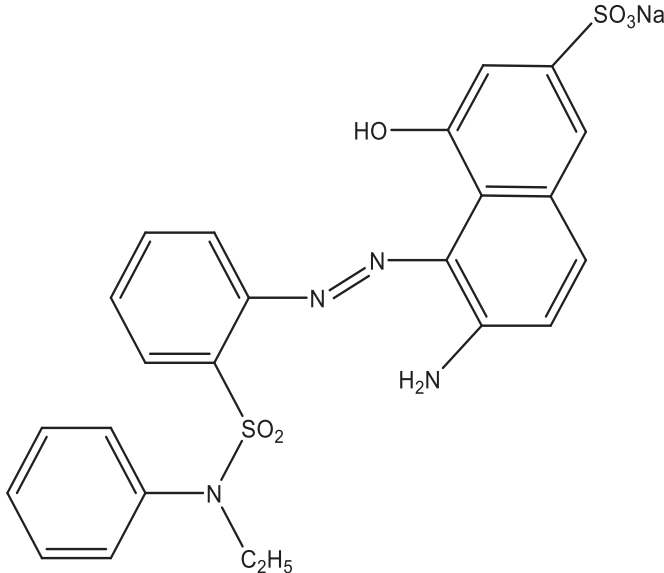
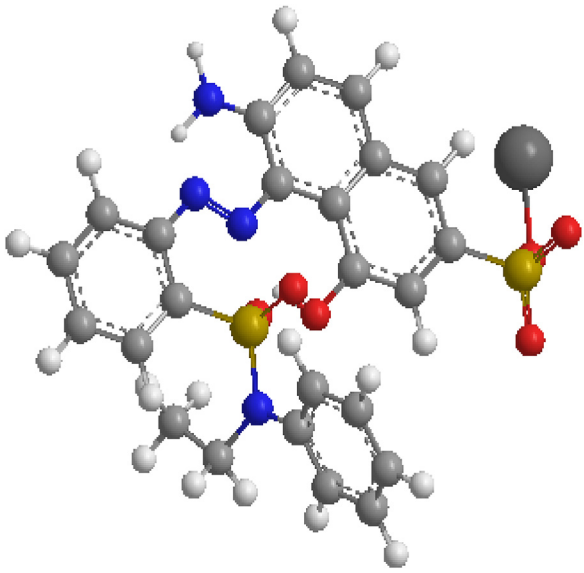
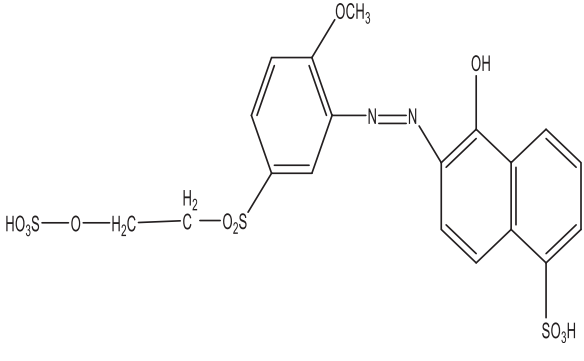
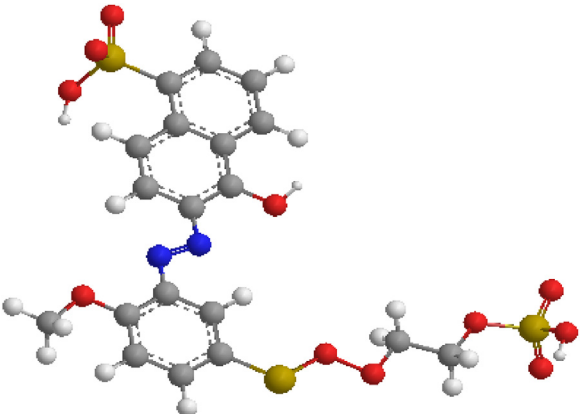
Parameter	Characteristic
Chemical name	sodium (E)-6-amino-5-((2-(N-ethyl-N-phenylsulfamoyl)phenyl)diazenyl)-4-hydroxynaphthalene-2-sulfonate
Type color	anionic
Chemical formula	$C_{24}H_{21}N_4NaO_6S_2$
Molecular weight (g/mol)	548.57
Wavelength of maximum absorption (nm)	512
Molar extinction coefficient, ϵ_{512} ($M^{-1} cm^{-1}$)	23,660
Chemical structure of color	
	

Table 2
Properties of the adsorbate (Remazol Red) used in the study.

Parameter	Characteristic
Chemical name:	6-((5-((ethylperoxy)thio)-methoxyphenyl)diazenyl)-5-hydroxynaphthalene-1-sulfonic acid compound with methyl hydrogen sulfate (1:1)
Type color	anionic
Chemical formula	$C_{20}H_{22}N_2NaO_{11}S_3$
Molecular weight (g/mol)	562.58
Wavelength of maximum absorption (nm)	541
Molar extinction coefficient, ϵ_{541} ($M^{-1} cm^{-1}$)	15,800
Chemical structure of color	
	

with initial dye concentration 1.22×10^{-3} M for AR57 and 1.06×10^{-3} M for RR and adsorbent dosage of 0.02 g ZnO. The solution was shaken at 200 rpm using shaker water bath for 30 min

and then the absorbance was measured spectrophotometrically.

The point of zero charge (pH_{PZC}) was determined by solid addition method [16]. A series of 0.1 M KNO_3 solutions (50 ML each)

were prepared and their pH values were adjusted in the range of 1.0–12.0 by addition of 0.1 mol L^{-1} HCl and 0.1 mol L^{-1} NaOH. To each solution, 0.1 g of ZnO nanoparticles was added and the suspensions were shaken manually and the solution was kept for a period of 48 h with intermittent manual shaking. The final pH of the solution was recorded and the difference between initial and final pH (ΔpH) (Y-axis) was plotted against the initial pH (X-axis). The point of this curve yielded pH_{PZC} .

3. Results and discussion

3.1. Characterization of ZnO nanoparticles

3.1.1. X-ray diffraction (XRD) patterns

The XRD patterns of the as-synthesized ZnO nanoparticles at different thermal treatment temperatures are shown in Fig. 1. The observed diffraction peaks connected with well crystallized ZnO indicate the formation of the hexagonal wurtzite structure with lattice constants $a = b = 3.249 \text{ \AA}$ and $c = 5.206 \text{ \AA}$ (space group P63mc, JCPDS card no. 36–1451) [17]. No additional peaks due to impurities were detected, indicating the high purity of the as-prepared ZnO. It can be seen that the XRD patterns of the ZnO samples are similar at different temperatures [18]. The peaks at $2\theta = 31.78, 34.43, 47.55, 56.62, 62.88, 67.97,$ and 69.11° can be attributed to the (100), (002), (101), (102), (110), (103), (112), and (201) planes of ZnO, respectively [19]. The crystallite size (D , \AA) of the ZnO nanoparticles was calculated by using the Scherrer formula Eq. (4).

$$D = K\lambda / \beta \cos \theta \quad (4)$$

where λ is the X-ray wavelength (1.54 \AA), β is the angular width of the peak at half its maximum intensity (full width at half-maximum) corrected for instrumental broadening, B is the maximum of the Bragg diffraction peak, and K is the Scherrer constant (0.9 \AA). The crystallite size of ZnO calculated from the high-intensity (101) peak was $208.98, 326.98,$ and 359.63 nm at the temperatures $450, 550,$ and 650°C , respectively. It can be easily concluded that by increasing the temperature, the average grain size increases [20] and the specific surface area decreases [21]. These results can be explained on the basis of the increased extent of agglomeration of the ZnO nanoparticles.

3.1.2. Fourier transform infrared (FTIR) analysis

The FTIR patterns of the as-synthesized ZnO nanoparticles at different thermal treatment temperatures are shown in Fig. 2. A broad peak observed at 3446 cm^{-1} corresponds to the vibrational

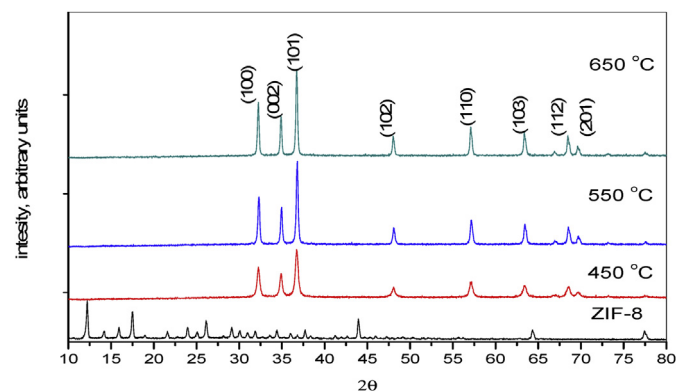


Fig. 1. X-ray diffraction spectra of ZIF-8 and ZnO nanoparticles at different temperatures 450, 550 and 650°C .

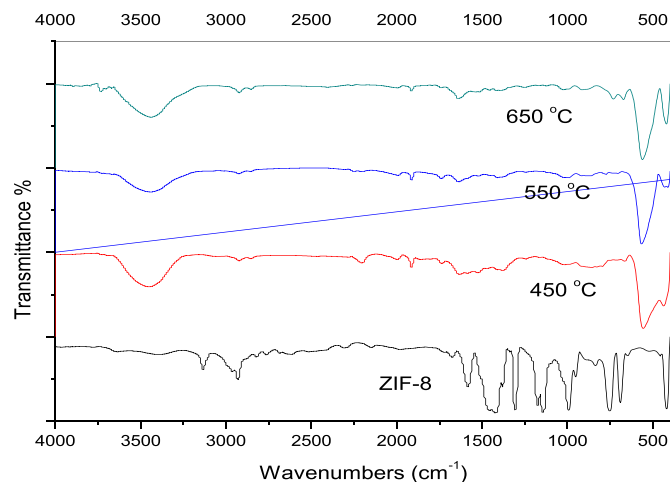


Fig. 2. FTIR spectrum of ZIF-8 and ZnO nanoparticles at different temperatures 450, 550 and 650°C .

modes of the O–H bond [22]. A relatively less intense peak at 1630 cm^{-1} represents the O–H stretching of the adsorbed water molecules. A very weak peak at $\sim 1918 \text{ cm}^{-1}$ is recognized as due to the symmetric C–H bond, which may be present because of the environmental conditions. The vibrations of ZnO are in the range $400\text{--}600 \text{ cm}^{-1}$. The band at 548 cm^{-1} is connected with oxygen deficiency and/or oxygen vacancy deficiency present in ZnO [23].

3.1.3. Brunauer-Emmett-Teller (BET) surface area

The BET surface area and Barrett–Joyner–Halenda (BJH) pore size of ZnO at 450°C were investigated using N_2 adsorption/desorption measurements at 77 K . The N_2 adsorption–desorption isotherm of ZnO nanoparticles can be classified as type III, which refers to the reversible isotherm is convex to the x axis over its entire range. It also indicates unrestricted multilayer formation process. It forms because lateral interactions between adsorbed molecules are strong in comparison to interactions between the adsorbent surface and adsorbate (Fig. 3).

The BET surface area for ZnO was $37.674 \text{ m}^2/\text{g}$ adopting a value of 16.2 \AA for the cross-sectional area of the N_2 molecule. However, the total pore volume taken at a saturation pressure and expressed as

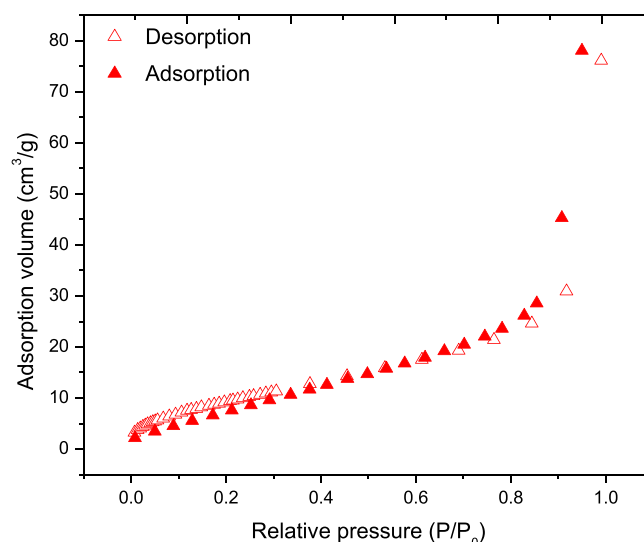


Fig. 3. N_2 sorption isotherm of ZnO nanoparticles at 450°C .

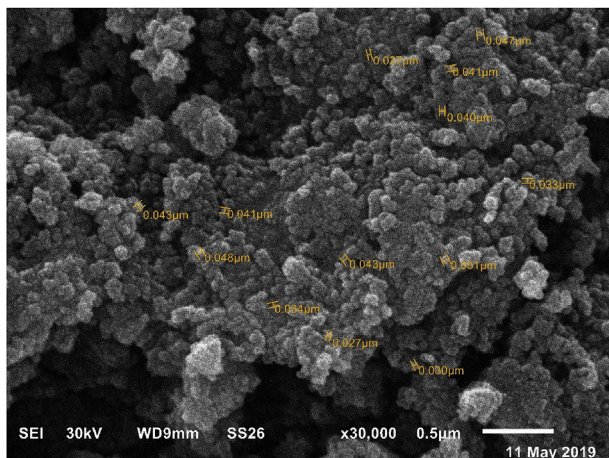


Fig. 4. SEM image of ZnO nanoparticles at 450 °C.

liquid volume is 0.1178 cm³/g and average pore diameter 12.5068 nm. The BJH surface area was 51.139 m²/g, pore volume 0.125 cm³/g and pore diameter Dv(d) 1.656 nm. The external surface area 37.674 m²/g were (calculated on t-plot method), which is beneficial for adsorption application [24].

3.1.4. SEM analysis

Structural characterization and morphology of ZnO was carried out through SEM analysis. Fig. 4 shows the SEM image of ZnO that prepared by calcination of ZIF-8 at 450 °C. SEM analysis approved that ZnO was nanoparticles as its average diameter was from 27 to 47 nm [25].

3.1.5. Energy-dispersive X-ray spectroscopy (EDX)

The energy dispersive X-ray analysis of ZnO nanoparticles at 450 °C was performed to know the elemental composition of zinc and oxygen (Fig. 5). The presence of carbon was observed in our study which was due to the use of ZIF-8, as a precursor for the synthesis of zinc oxide nanoparticles [26].

3.2. Batch experiments

3.2.1. Determination of point of zero charge (pH_{PZC})

pH was one of the most important parameters for AR57 and RR sorption, as it determined which ionic species were present in the adsorbate solution and the surface charge of the sorbent. Surface

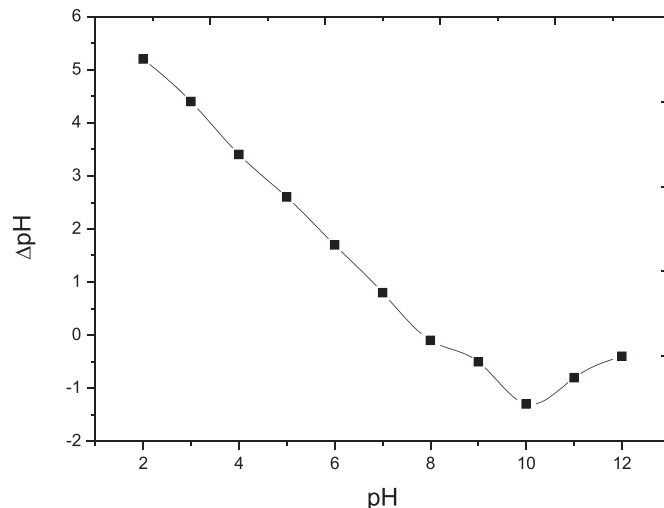


Fig. 6. Relation between the initial pH and ΔpH of ZnO nanoparticles at 450 °C.

charge of the ZnO nanoparticles was determined by the PZC, which is defined as the pH (pH_{PZC}) at which the positive charges on the surface equal the negative charges [16]. The pH_{PZC} of ZnO was found to be 7.88. This shows that below this pH, the ZnO nanoparticles acquires a positive charge due to protonation of functional groups and above this pH, negative charge exists on the surface of ZnO. The adsorption of anionic dyes is favored at pH < pH_{PZC} where the surface becomes positively charged (Fig. 6).

3.2.2. Effect of pH

The pH value of aqueous solution is an important parameter in the adsorption study of anionic dyes because of its effect on both ionization of dye molecules and surface binding sites. The removal of the tested dyes AR57 and RR by ZnO nanoparticles at different pH values (2–12) was studied at initial concentration of 1.22 × 10⁻³ M and 1.06 × 10⁻³ M for AR57 and RR, respectively on 0.02 g ZnO at 25 °C. ZnO nanoparticles has proved to be an effective adsorbent for the removal of these dyes and the most effective pH was 2 for AR57 and 3 for RR and it was used in further studies (Fig. 7).

This indicate that the adsorption is highly dependent on pH of the solution which affects the surface charge of the adsorbent and the degree of ionization and speciation of adsorbate [27,28]. At lower pH more protons will be available, thereby increasing electrostatic attractions between negatively charged dye anions and positively charged adsorption sites and causing an increase in dye

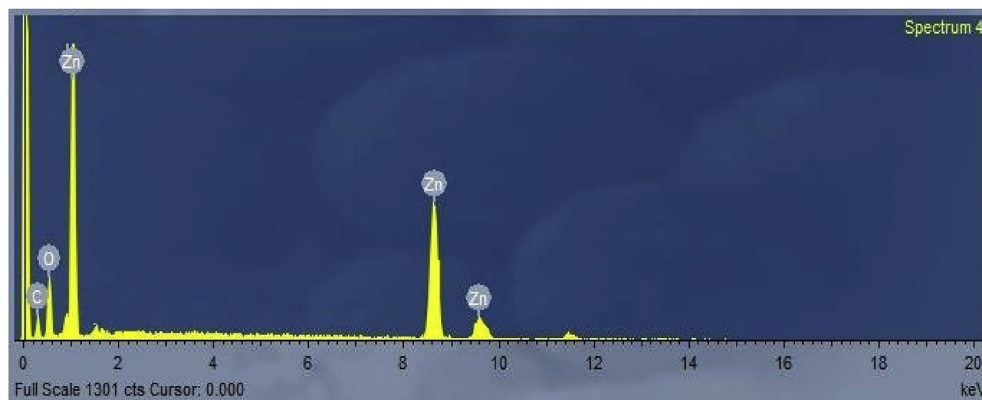


Fig. 5. EDX spectrum of ZnO nanoparticles at 450 °C.

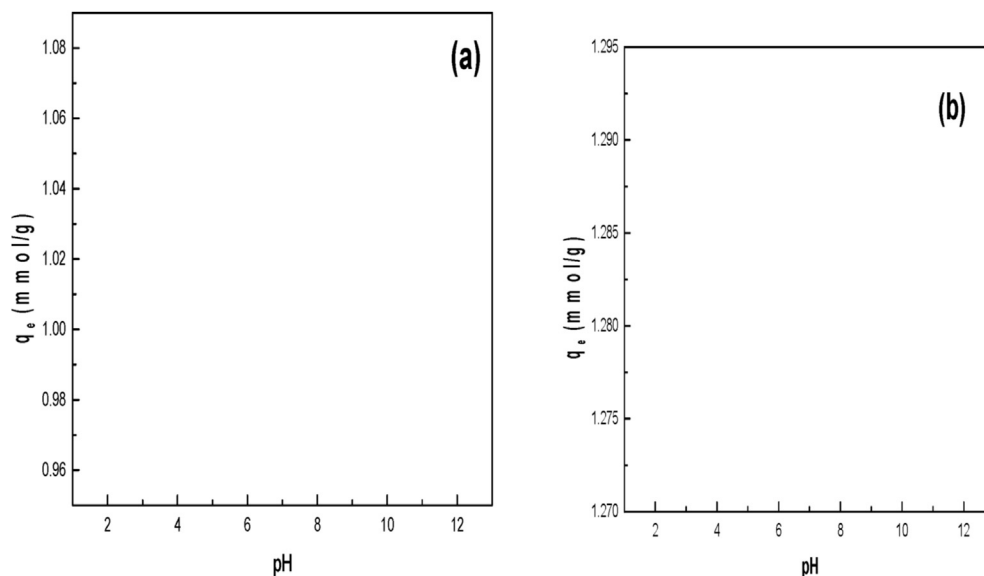


Fig. 7. (a) pH effect on AR57 adsorption using ZnO nanoparticles at 450 °C as adsorbent (T: 25 °C; C_0 : 1.22×10^{-3} M). (b) pH effect on RR adsorption using ZnO nanoparticles at 450 °C as adsorbent (T: 25 °C; 1.06×10^{-3} M).

adsorption [13]. The high adsorption capacity is due to the strong electrostatic interaction between the Zn^{2+} and SO_3^- dye anions. When the pH of the solution is increased, the positive charge on the oxide or solution interface decreases and the adsorbent surface appears negatively charged. On the contrary, a lower adsorption at higher pH values may be due to the abundance of OH^- ions and because of ionic repulsion between the negatively charged surface and the anionic dye molecules. There are also no exchangeable anions on the outer surface of the adsorbent at higher pH values and consequently the adsorption decreases [29,30]. The pH_{PZC} of ZnO nanoparticles was found to be 7.88. So, the adsorption of anionic dyes is favored at $pH < pH_{PZC}$ where the surface becomes positively charged.

3.2.3. Effect of adsorbent dosage

The adsorption of AR57 and RR on the ZnO nanoparticles sorbent was studied at 25 °C by changing the quantity of adsorbent range of (0.01–0.1 g) per 25 mL, at adsorbate concentration 1.22×10^{-3} M and pH 2 for AR57 while for RR concentration

1.06×10^{-3} M and pH 3. The results in Figs. 8a and 9a show the AR57 and RR adsorption capacity as a function of adsorbent amount. It has been found that the adsorption capacity decreases from 1.06 to 0.28 mmol/g and 2.59 to 0.26 mmol/g for AR57 and RR, respectively when the dosage of ZnO increases from 0.01 to 0.1 g per 25 mL. Figs. 8b and 9b show the effect of dosage on the equilibrium concentration (C/C_0) of AR57 and RR by the zinc oxide sorbent. As the dosage increases, the equilibrium concentration of AR57 and RR is decreased, which is due to the increase in the adsorbent surface area of the adsorbent. The results shown indicate that the removal efficiency increases up to 92.1% ($C/C_0 = 0.079$) at adsorbent dose of 0.1 g per 25 mL for AR57, while for RR the removal efficiency increases up to 99.3% ($C/C_0 = 0.0065$) at adsorbent dosage of 0.1 g per 25 mL. The surface of the adsorbent is composed of active sites with a spectrum of binding energies [31]. At the low dose of adsorbent, all of the sites are exposed entirely and the adsorption on the surface is saturated faster showing a higher adsorption capacity. An increase in the mass of adsorbent leads to a decrease in equilibrium adsorption capacity per unit

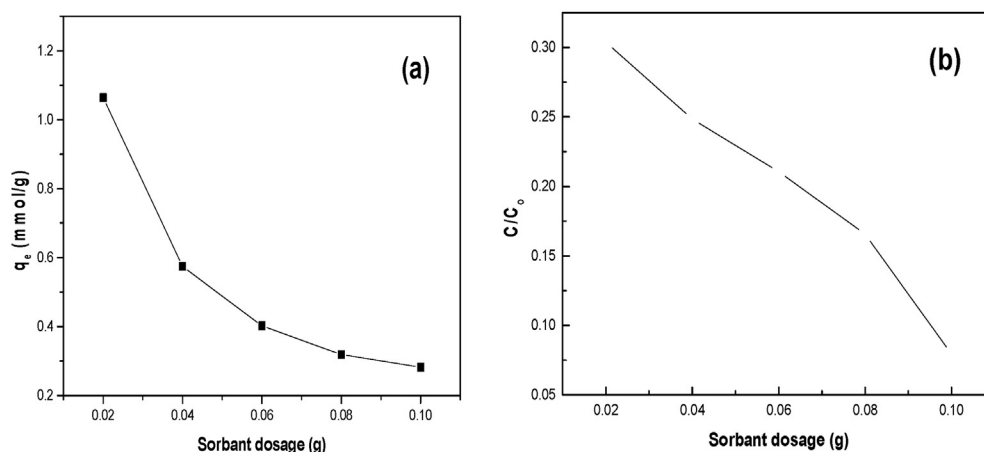


Fig. 8. Effect of sorbent dose (SD) on AR57 adsorption using ZnO nanoparticles at 450 °C: (a) Sorption capacity vs. SD, (b) Relative residual concentration (C/C_0) vs. SD (C_0 : 1.2×10^{-3} M; T: 25 °C; pH 2).

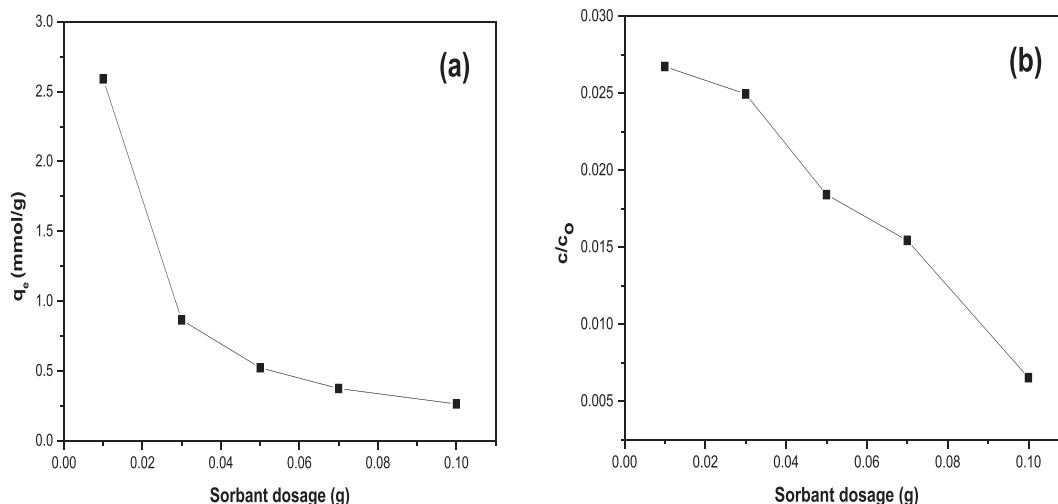


Fig. 9. Effect of sorbent dosage (SD) on RR adsorption using ZnO nanoparticles at 450 °C: (a) Sorption capacity vs. SD, (b) Relative residual concentration (C/C_0) vs. SD (C_0 : 1.2×10^{-3} M; T: 25 °C; pH 3).

weight of the adsorbent (q_e) because there is excess adsorbent for the limited amount of AR57 and RR ions in the solution. According to the result, the dose of 0.01 g per 25 mL will achieve the maximum loading capacity for the sorbent, and the dose of 0.1 g per 25 mL will achieve the maximum removal efficiency 92.1% ($C/C_0 = 0.079$) for AR57 and 99.3% ($C/C_0 = 0.0065$) for RR. So the determination of the optimum adsorbent dose depends on the design and purpose of treatment process.

3.2.4. Effect of adsorbent particle size on dye removal

The influence of crystalline size of ZnO nanoparticles (adsorbent) on adsorption of AR57 and RR was tested using different particle size of ZnO (208.98, 326.98 and 359.63 nm) as its the size of ZnO at different temperature of calcination 450, 550, 650 °C, respectively. The adsorbent dosage was 0.02 g; volume of the dye solution was 25 mL, Concentration 1.22×10^{-3} M pH 2 for AR57 and concentration 1.06×10^{-3} M pH 3 for RR, shaking speed of 200 rpm.

The percentage adsorption of AR57 decreased from 99.8 > 83.79 > 82.23% on increasing the particle size (208.98, 326.98 and 359.63 nm) while RR The percentage of its adsorption was decreased from 99.78 > 93.98 > 92.18% on increasing the particle size (Fig. 10). The higher adsorption for AR57 and RR onto smaller particle size of the adsorbent ZnO at 450 °C was attributed to increased accessibility of binding sites to increased surface area for bulk adsorption of the dye [32].

3.2.5. Effect initial concentration (C_0)

The influence of initial concentration of AR57 and RR onto ZnO nanoparticles at 450 °C was investigated with dye concentration 8.85×10^{-4} – 3.63×10^{-3} M range for AR57 while 3.7×10^{-5} – 1.06×10^{-3} M range for RR and adsorbent dosage of 0.02 g. The percentage (%) removal decreased with increase of initial dye concentration of AR57 and RR [33]. The percentage decrease in adsorption is ascribed to saturation of the active binding sites of

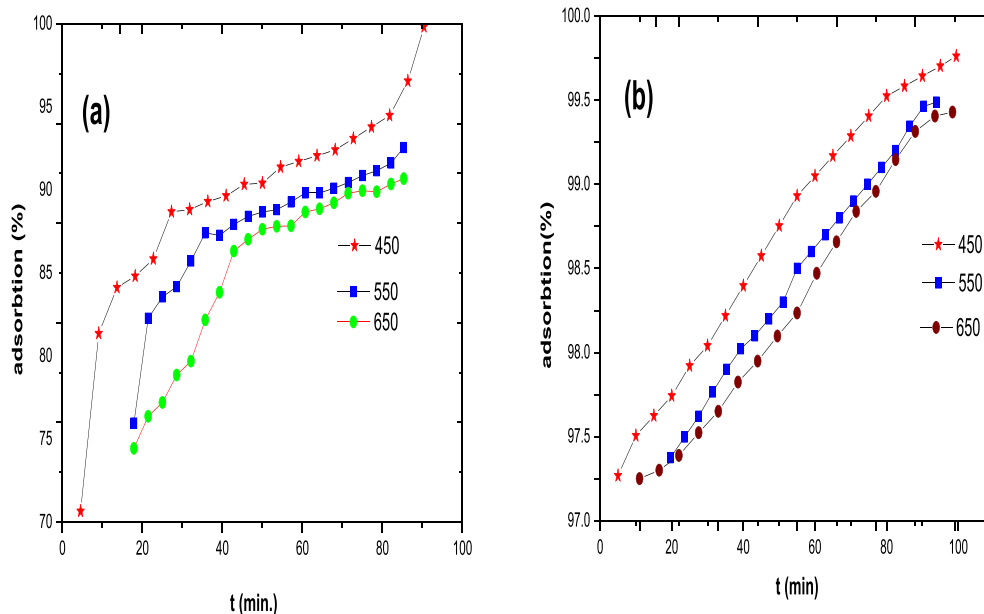


Fig. 10. Effect of particle size of ZnO nanoparticles on the adsorption of AR57 (a) and RR (b).

ZnO at higher concentrations of AR57 and RR.

3.2.6. Adsorption isotherms

Isotherm studies give significant insights by clarifying the adsorbate distribution between solid and solution phase during the adsorption equilibrium, and adsorption isotherms reveal the behavior of adsorbate how to interact with adsorbent [34]. Equilibrium studies that give the capacity of the adsorbent and adsorbate are described by adsorption isotherms, which is usually the ratio between the quantity adsorbed and that remained in solution at equilibrium at fixed temperature. Various isotherm models have been used for considering the equilibrium adsorption of compounds from solutions such as Langmuir [35,36], Freundlich [37], Dubinin–Radushkevich [38] and Temkin [39].

The Langmuir isotherm model assumes the uniform energies of adsorption onto the adsorbent surface. It is based on assumption of the existence of monolayer adsorption onto a completely homogeneous surface with a finite number of identical sites and with negligible interaction between adsorbed molecules [35]. The Freundlich model is an empirical equation based on adsorption of heterogeneous surface or surface supporting sites of varied affinities. It is assumed that the stronger binding sites are occupied first and that the binding strength decreases with the increasing degree of site occupation [37]. Dubinin–Radushkevich isotherm is an empirical model initially for the adsorption of subcritical vapors onto micropore solids following a pore filling mechanism. It is applied to distinguish the physical and chemical adsorption for removing a molecule from its location in the sorption space to the infinity [38]. The Temkin isotherm assumes that the heat of adsorption of all molecules in the phase decreases linearly when

the layer is covered and that the adsorption has a maximum energy distribution of uniform bond [39].

The linear and nonlinear forms of Langmuir, Freundlich, Dubinin–Radushkevich and Temkin isotherm models and their parameters are shown in Tables 3 and 4, for AR57 and RR respectively where q_e the adsorbed amount of dye at equilibrium concentration (mmol.g^{-1}), q_{mL} is the maximum sorption capacity (corresponding to the saturation of the monolayer, mmol.g^{-1}) and K_L is the Langmuir binding constant which is related to the energy of sorption (L.mmol^{-1}), C_e is the equilibrium concentration of dyes in solution (M). K_F (mmol.g^{-1}) (L.mmol^{-1}) $^{1/n}$ and n are the Freundlich constants related to the sorption capacity and intensity, respectively. K_{DR} ($\text{J}^2 \text{mol}^{-2}$) is a constant related to the sorption energy, q_{DR} (mmol g^{-1}) is the theoretical saturation capacity, ϵ ($\text{J}^2 \text{mol}^{-2}$) is the Polanyi potential. R ($8.314 \text{ Jmol}^{-1} \text{K}^{-1}$) is the gas constant, T is the temperature where the adsorption occurs, A_T (L mg^{-1}) is the Temkin isotherm constant, b_T (J mol^{-1}) is Temkin constant in relation to heat of adsorption.

The Langmuir isotherm model was found to be the most suitable model for describing the isotherm for the adsorption of both AR57 and RR dyes into the ZnO sorbent Figs. 11 and 12. However, from the isotherm fitting, the Freundlich lines deviated from the experimental data points. The isotherm fitting was plotted on the basis of the nonlinear equations using the model constant parameters obtained from the linear equation plot analysis. The Langmuir model presented the high correlation coefficient $R^2 = 0.9999$ for AR57 and RR was 0.99952.

In addition, the q_m calculated from the Langmuir isotherm was close to the experimental q_{max} . Analysis of isotherm parameters proposed by Dubinin–Radushkevich was calculated (Tables 3 and 4)

Table 3
Isotherms and their linear forms for the adsorption of AR57 onto ZnO.

Isotherm	Equation		Value of parameters	
Langmuir	$\frac{C_e}{q_e} = \frac{1}{q_m K_L} + \frac{C_e}{q_m}$	The constants q_m and K_L are calculated by the plot of C_e/q_e vs. C_e with slope $1/q_m$ and intercept $1/(q_m K_L)$	$q_{m \text{ exp}}$ (mmol.g^{-1}) q_m (mmol.g^{-1}) K_L (Lmmol^{-1}) R^2	1.3675 1.3811 248387.968 0.9999
Freundlich	$\ln q_e = \ln K_F + \frac{1}{n} \ln C_e$	K_F and n can be calculated from a linear plot of $\ln q_e$ vs. $\ln C_e$	n K_F (mmol.g^{-1}) (Lmmol^{-1}) $^{1/n}$ R^2	13.56852 0.77284 0.86585
Dubinin–Radushkevich	$\ln q_e = \ln Q_{DR} - K_{DR} \epsilon^2$	The slope of the plot of $\ln q_e$ vs. ϵ^2 gives K_{DR} (mol^2/kJ^2) and the intercept yields the adsorption capacity, Q_{DR} (mmol/g)	Q_{DR} K_{DR} ($\text{J}^2 \text{mol}^{-2}$) E_a (kJmol^{-1}) R^2	0.50744 −8.18E-10 24.7 0.90394
Temkin	$q_e = \beta_T \ln K_T + \beta_T \ln C_e$	The parameters β and K_T are the Temkin constants that can be determined by the plot of q_e vs. $\ln C_e$	b_T (Lmol^{-1}) A_T (kJmol^{-1}) R^2	27.670 21.474 0.89075

Table 4
Isotherms and their linear forms for the adsorption of RR onto ZnO.

Isotherm	Equation		Value of parameters	
Langmuir	$\frac{C_e}{q_e} = \frac{1}{q_m K_L} + \frac{C_e}{q_m}$	The constants q_m and K_L are calculated by the plot of C_e/q_e vs. C_e with slope $1/q_m$ and intercept $1/(q_m K_L)$	$q_{m \text{ exp}}$ (mmol.g^{-1}) q_m (mmol.g^{-1}) K_L (Lmmol^{-1}) R^2	1.26 1.26 648744.87 0.99952
Freundlich	$\ln q_e = \ln K_F + \frac{1}{n} \ln C_e$	K_F and n can be calculated from a linear plot of $\ln q_e$ vs. $\ln C_e$	n K_F (mmol.g^{-1}) (Lmmol^{-1}) $^{1/n}$ R^2	1.519 2.2414 0.77376
Dubinin–Radushkevich	$\ln q_e = \ln Q_{DR} - K_{DR} \epsilon^2$	The slope of the plot of $\ln q_e$ vs. ϵ^2 gives K_{DR} (mol^2/kJ^2) and the intercept yields the adsorption capacity, Q_{DR} (mmol/g)	Q_{DR} K_{DR} ($\text{J}^2 \text{mol}^{-2}$) E_a (kJmol^{-1}) R^2	0.4926 −5.488E-10 30.185 0.79887
Temkin	$q_e = \beta_T \ln K_T + \beta_T \ln C_e$	The parameters β and K_T are the Temkin constants that can be determined by the plot of q_e vs. $\ln C_e$	b_T (Lmol^{-1}) A_T (kJmol^{-1}) R^2	34704.75 26.3697 0.76632

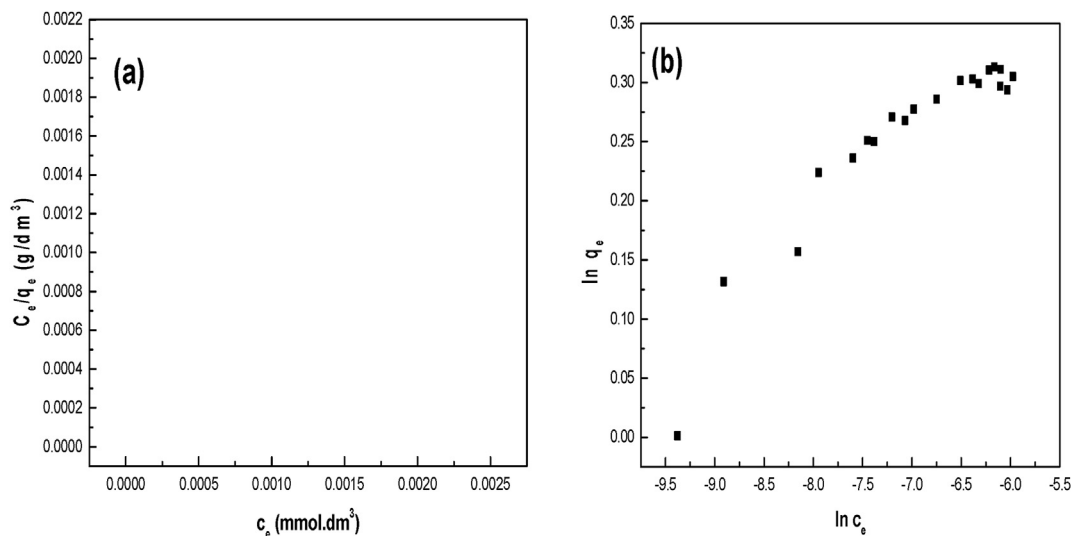


Fig. 11. Linearized plots for sorption isotherms for AR57: (a) Langmuir equation, (a) Freundlich equation.

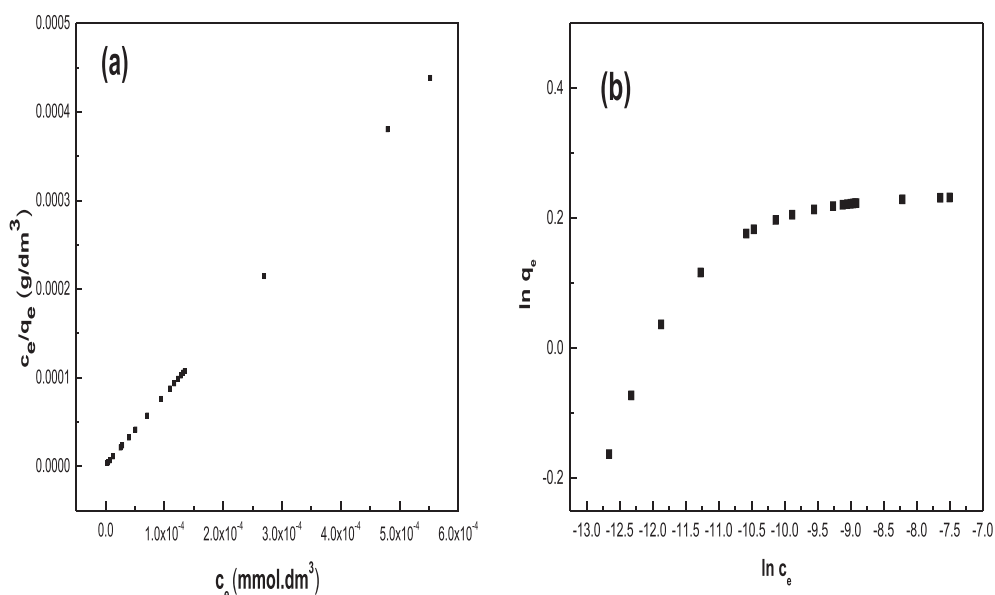


Fig. 12. Linearized plots for sorption isotherms for RR: (a) Langmuir equation, (b) Freundlich equation.

for both AR57 and RR. This isotherm was developed taking into account the effect of the porous structure of the sorbent, and the energy involved in the sorption process. The results of Dubinin-Radushkevich isotherm are reported in Table 3 and Fig. 13 for AR57 and Table 4 and Fig. 14 for RR. The value of the mean energy of sorption is 24.70 and 30.185 kJ mol⁻¹ for AR57 and RR, respectively: this is dependable with the proposed mechanism of chemisorption. Indeed, it is generally admitted that 8 kJ mol⁻¹ is the limit energy for distinguishing, physical (below 8 kJ mol⁻¹) and chemical sorption (up 8 kJ mol⁻¹).

A comparison of the correlation coefficient values obtained from the Langmuir, Freundlich, Dubinin-Radushkevich and Temkin isotherm models (Tables 3 and 4), reveals that the correlation coefficients for the Langmuir isotherm are higher than those for the Freundlich, Dubinin-Radushkevich and Temkin isotherm models. This result suggests that the binding of dye ions may occur as a monolayer on the surface of the sorbent and that the uptake occurs

on a homogenous surface by monolayer sorption. The presence the same type of functional groups is comforting the hypothesis of homogeneous surface (or homogeneous energies of sorption). The ranking of the models as follow: Langmuir > Temkin > Freundlich > Dubinin-Radushkevich for AR57 while for RR Langmuir > Dubinin-Radushkevich > Temkin > Freundlich.

3.2.7. Adsorption kinetics and mechanism studies

The study of adsorption kinetics describes the solute uptake rate and evidently this rate controls the residence time of adsorbate uptake at the solid-solution interface. The rate of removal of tested dye by adsorption was rapid initially and then slowed gradually until it attained an equilibrium beyond which there was significant increase in the rate of removal. The maximum adsorption was observed at 100 min and it is thus fixed as the equilibrium time.

Aiming at evaluating the adsorption kinetics of tested dyes onto ZnO, the pseudo-first-order and pseudo-second-order kinetic

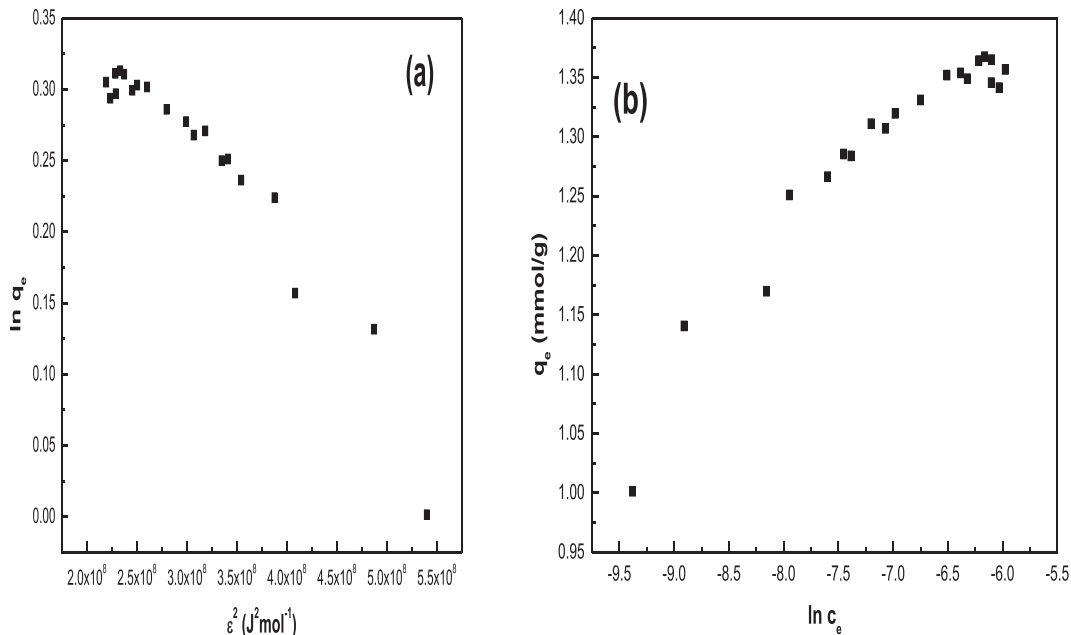


Fig. 13. Linearized plots for sorption isotherms for AR57: (a) Dubbin-Radushkevich equation, (b) Temkin model.

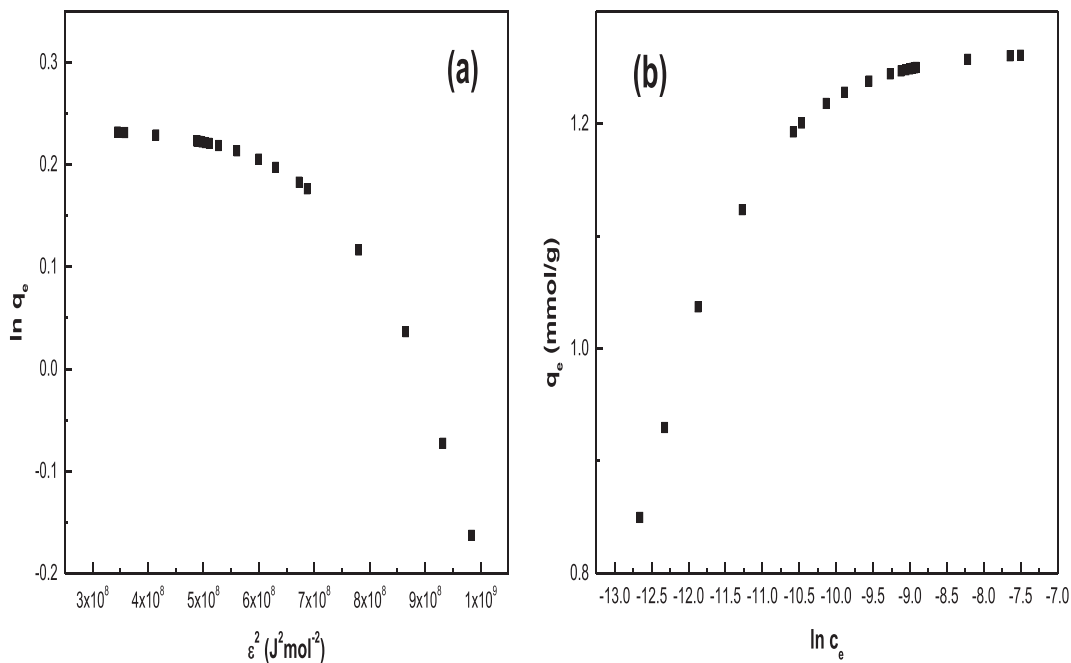


Fig. 14. Linearized plots for sorption isotherms for RR: (a) Dubbin-Radushkevich equation, (b) Temkin model.

models were used to fit the experimental data, according to the below kinetic model equations.

The pseudo-first-order rate expression of Lagergren [40] is given as Eq. (5):

$$\log(q_e - q_t) = \log q_e - k_1 t \tag{5}$$

The pseudo-second-order kinetic model [41] is expressed as Eq. (6):

$$t / q_t = 1/k_2 q_2^2 + 1/q_2 t \tag{6}$$

where q_t is the amount of dye adsorbed (mg.g^{-1}) at various times t , q_e is the maximum adsorption capacity (mg.g^{-1}) for pseudo-first-order adsorption, k_1 is the pseudo-first-order rate constant for the adsorption process (min^{-1}), q_2 is the maximum adsorption capacity (mg.g^{-1}) for the pseudo-second-order adsorption, k_2 is the rate constant of pseudo-second-order adsorption ($\text{g.mol}^{-1}.\text{min}^{-1}$). The straight-line plots of $\log(q_e - q_t)$ vs. t for the pseudo-first-order

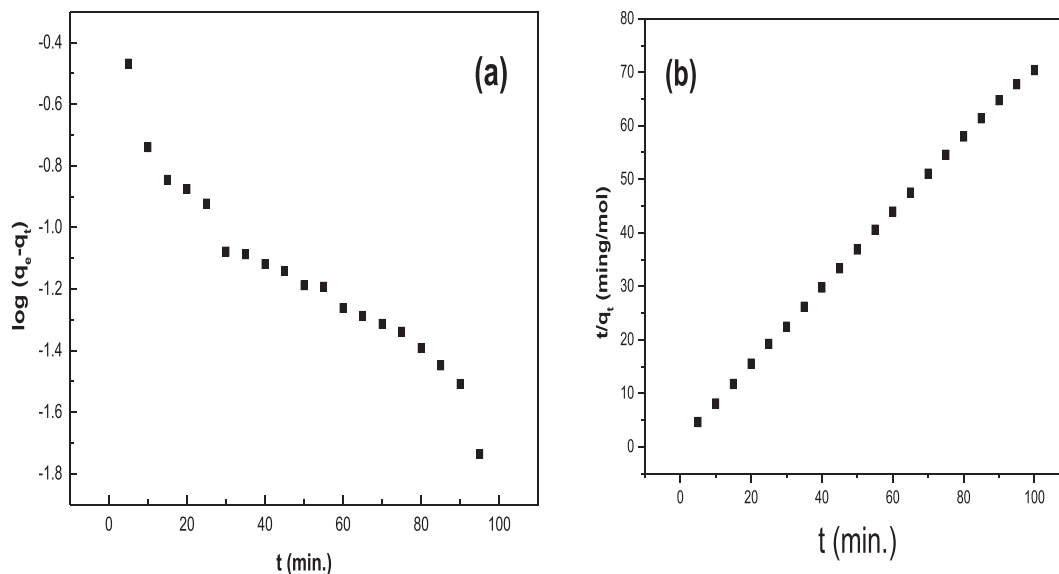


Fig. 15. Modeling of uptake kinetics for AR57 with: (a) pseudo-first-order rate expression, (b) pseudo-second-order rate expression.

reaction and t/q_t vs. t for the pseudo-second-order reaction Figs. 15 and 16 for the adsorption of tested dyes onto (ZnO) have also been tested to obtain the rate parameters. The k_1 , k_2 , q_e , q_2 , and correlation coefficients, r_1^2 and r_2^2 for the dye under different temperatures were calculated from these plots and are given in Tables 5 and 6.

Since neither the pseudo-first-order nor the pseudo-second-order model can identify the diffusion mechanism, the kinetic results were further analyzed for diffusion mechanism by using the intra-particle diffusion model. The effect of intra-particle diffusion constant (internal surface and pore diffusion) on adsorption can be determined by the following Eq. (7).

$$q_t = k_{id}t^{1/2} + I \quad (7)$$

where I is the intercept and k_{id} is the rate constant of intra-particle diffusion ($\text{mg g}^{-1} \text{min}^{0.5}$) which is determined from the linear plot of q_t vs. $t^{1/2}$ (Figs. 17 and 18) and it is usually used to compare mass

transfer rates. According to this model, the plot of uptake, q_t , vs. the square root of time, $t^{1/2}$ should be linear if intra-particle diffusion is involved in the adsorption process and if these lines pass through the origin, then intra-particle diffusion is the rate controlling step. The intra-particle diffusion rate constant and intercept values are displayed in (Tables 5 and 6).

The Elovich equation is used for general application to chemical adsorption [42]. The equation has been applied satisfactorily to some chemical adsorption processes and has been found to cover a wide range of slow adsorption rates. The same equation is often valid for systems in which the adsorbing surface is heterogeneous Eq. (8), and is formulated as:

$$q_t = (1/\beta)\ln(\alpha\beta) + (1/\beta)\ln t \quad (8)$$

where α is the chemical adsorption rate (mg/mg min) and β is a coefficient in relation with the extension of covered surface and activation energy of chemical adsorption (g/mg). Plot of q_t vs. $\ln t$ gave a linear relationship with slope of $(1/\beta)$ and an intercept of $(1/\beta)\ln(\alpha\beta)$.

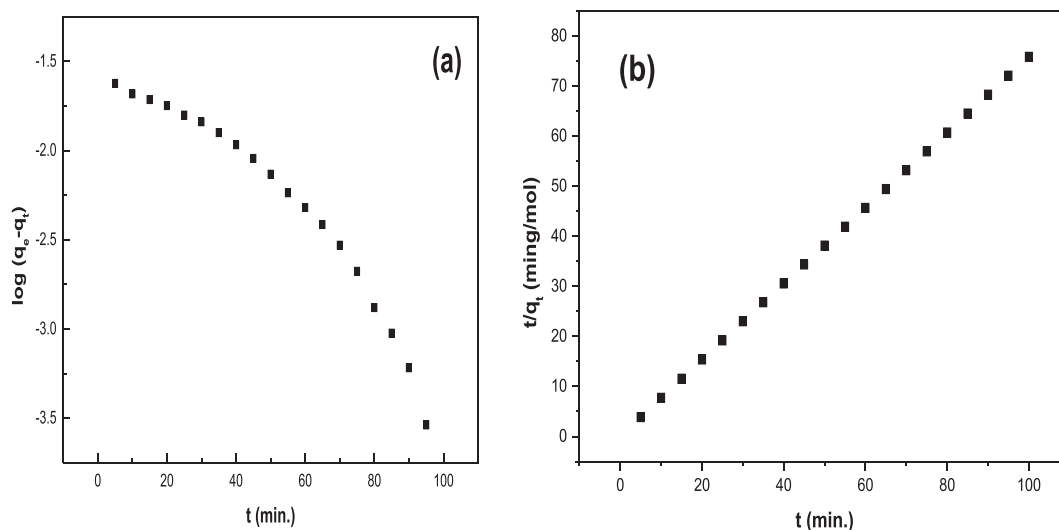


Fig. 16. Modeling of uptake kinetics for RR with: (a) pseudo-first-order rate expression, (b) pseudo-second-order rate expression.

Table 5
Kinetic parameters and their correlation coefficients for the adsorption of AR57 onto ZnO.

Model	Equation		Value of parameters	
Pseudo-First-order kinetic	$\log(q_e - q_t) = \log q_e - \left(\frac{K_1}{2.303}\right)t$	The plot of $\ln(q_e - q_t)$ against t gives a straight line with the slope $-K_1$ and intercept $\ln q_e$	K_1 (min^{-1})	0.64906
Pseudo-second-order kinetic	$\frac{t}{q_t} = \frac{1}{K_2 q_e^2} + \frac{t}{q_e}$	Values of K_2 and q_e for different initial concentrations of dye were calculated from the slope and intercept of the linear plot of t/q_t vs. t	q_e (mmol g^{-1})	-0.01
			R^2	0.91946
			K_2 ($\text{g mg}^{-1} \text{min}^{-1}$)	0.3245
Intraparticle diffusion	$q_t = K_i t^{1/2} + X$	The parameters K_{dif} and C were determined from the linear plot of q_t vs. $t^{1/2}$	q_e (mmol g^{-1})	1.424
			R^2	0.99956
			K_i ($\text{mg g}^{-1} \text{min}^{1/2}$)	-0.0574
Elovich	$q_t = \frac{1}{\beta} \ln(\alpha\beta) + \frac{1}{\beta} \ln t$	The constants α and β were obtained from the slope and intercept of a line plot of q_t vs. $\ln t$	X (mg g^{-1})	0.46639
			R^2	0.25947
			β (g/mg)	-4.9596
Experimental data			α ($\text{mg g}^{-1} \cdot \text{min}^{-1}$)	2.28
			R^2	0.4365
			q_e (exp) (mmol g^{-1})	1.4

Table 6
Kinetic parameters and their correlation coefficients for the adsorption of RR onto ZnO.

Model	Equation		Value of parameters	
Pseudo-First-order kinetic	$\log(q_e - q_t) = \log q_e - \left(\frac{K_1}{2.303}\right)t$	The plot of $\ln(q_e - q_t)$ against t gives a straight line with the slope $-K_1$ and intercept $\ln q_e$	K_1 (min^{-1})	1.31246
Pseudo-second-order kinetic	$\frac{t}{q_t} = \frac{1}{K_2 q_e^2} + \frac{t}{q_e}$	Values of K_2 and q_e for different initial concentrations of dye were calculated from the slope and intercept of the linear plot of t/q_t vs. t	q_e (mmol g^{-1})	0.11809
			R^2	0.92016
			K_2 ($\text{g mg}^{-1} \text{min}^{-1}$)	0.67807
Intraparticle diffusion	$q_t = K_i t^{1/2} + X$	The parameters K_{dif} and C were determined from the linear plot of q_t vs. $t^{1/2}$	q_e (mmol g^{-1})	1.32188
			R^2	0.99975
			K_i ($\text{mg g}^{-1} \text{min}^{1/2}$)	-0.0609
Elovich	$q_t = \frac{1}{\beta} \ln(\alpha\beta) + \frac{1}{\beta} \ln t$	The constants α and β were obtained from the slope and intercept of a line plot of q_t vs. $\ln t$	X (mg g^{-1})	0.48581
			R^2	0.18906
			β (g/mg)	-4.571
Experimental data			α ($\text{mg g}^{-1} \cdot \text{min}^{-1}$)	2.4136
			R^2	0.34325
			q_e (exp) (mmol g^{-1})	1.1295

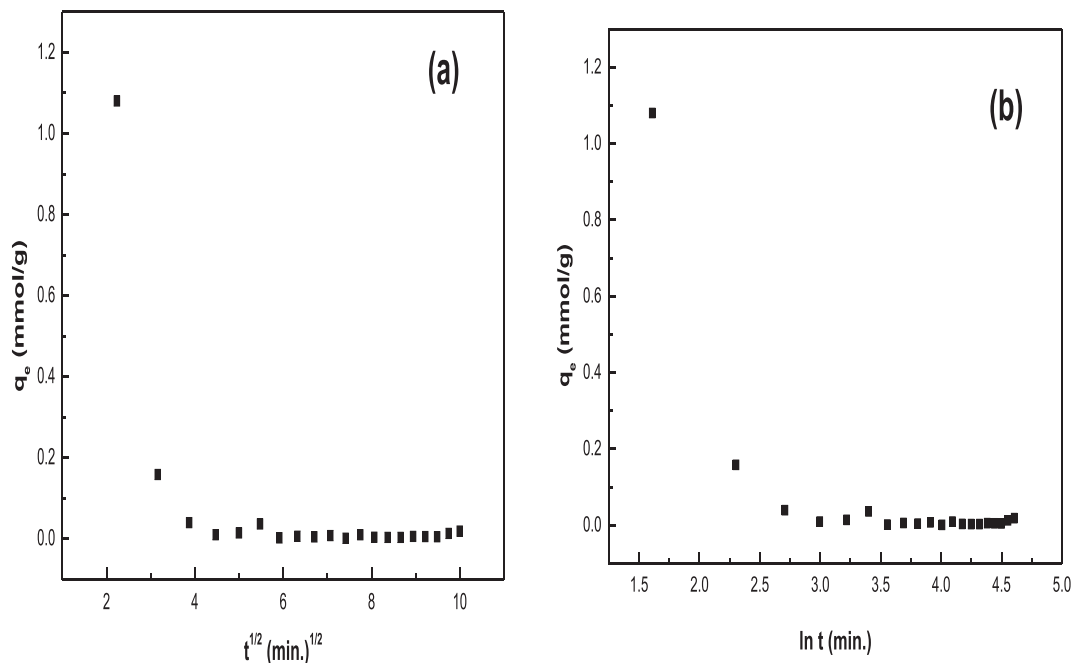


Fig. 17. Modeling of uptake kinetics for AR57 with (a) simplified model of resistance to intraparticle diffusion (Morris and Weber equation), (b) Elovich equation.

β) $\ln(\alpha\beta)$. The $1/\beta$ value reflects the number of sites available for adsorption whereas the value of $(1/\beta) \ln(\alpha\beta)$ indicates the adsorption quantity when $\ln t$ equal to zero.

Since neither the pseudo-first-order nor the pseudo-second-order model can identify the diffusion mechanism, the kinetic

results were further analyzed for diffusion mechanism by using the intra-particle diffusion model. The effect of intra-particle diffusion constant (internal surface and pore diffusion) on adsorption can be determined by the following Eq. (9).

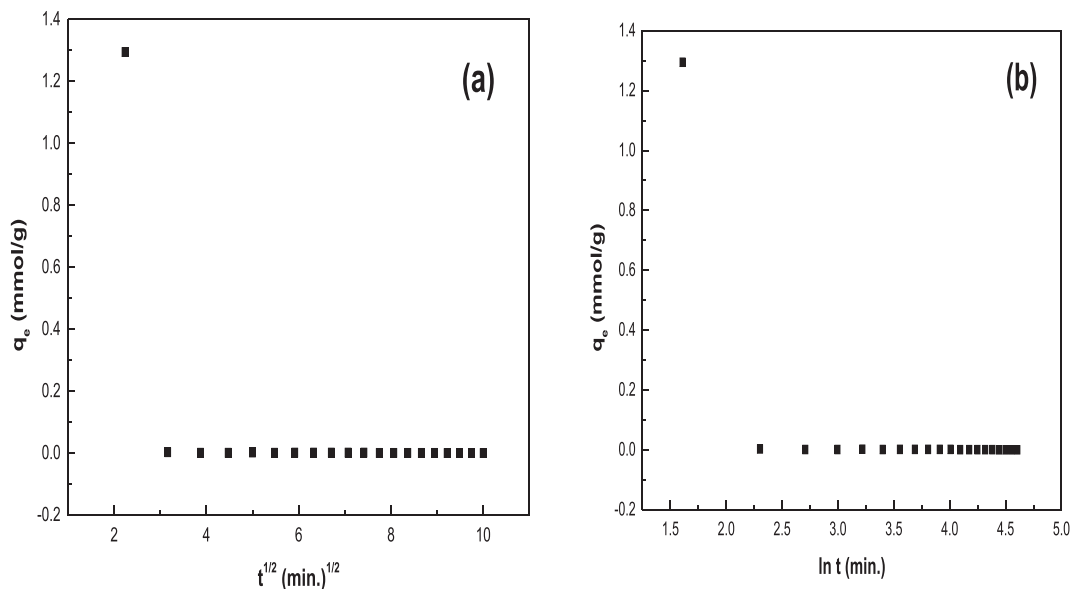


Fig. 18. Modeling of uptake kinetics for RR with (a) simplified model of resistance to intraparticle diffusion (Morris and Weber equation), (b) Elovich equation.

$$q_t = k_{id}t^{1/2} + I \quad (9)$$

Upon comparison among the kinetic models, the R^2 values of the pseudo-second-order kinetic model (0.99975) are much higher than those of pseudo-first-order kinetic model (0.9202) for AR57 while for RR the R^2 values of the pseudo-second-order kinetic model (0.99956) are much higher than those of pseudo-first-order kinetic model (0.91946), implying that the kinetics of both of dyes adsorption follows the pseudo-second-order kinetic model. This consideration is confirmed by the correlation coefficients and the q_e (calc.) value from the pseudo-second-order kinetic model is in good agreement with the experimental results. The rate-limiting step in this adsorption process may be chemisorption involving strong forces through the sharing or exchanging of electrons between sorbent and sorbate [18]. The intra-particle diffusion curve gives multilinearity, it does not pass through the origin. The intra-particle diffusion kinetic model ($R^2 = 0.259$ and 0.18906) for AR57 and RR, respectively was calculated from the slope of the corresponding second linear region Figs. 17 and 18. It is assumed that the external resistance to mass transfer surrounding the particles is significant only in the initial stages of adsorption (initial sharp increase). The second linear portion is the gradual adsorption stage with controlling intraparticle diffusion. When the plots do not pass through the origin, indicates that the pore diffusion is not the sole rate-limiting step but also other kinetic models may control the rate of adsorption, all of which may be operating simultaneously [43]. The Elovich equation assumes that the active sites of the adsorbent are heterogeneous and therefore, exhibit different activation energies for chemisorption. When increasing the concentration of dye, it was observed that the constant α (related to the rate of chemisorption) increased and the constant β (related to the surface coverage) decreased (Tables 5 and 6), which is due to the decrease in the available adsorption surface for the adsorbates. Therefore, by increasing the concentration, within the range studied, the rate of chemisorption can be increased [44].

Therefore, the adsorption kinetics can be satisfactorily approximated by the pseudo-second-order kinetic model, based on the assumption that the rate-limiting step may be chemisorption involving electrostatic forces through the sharing or exchange of electrons between the adsorbent and the adsorbate.

The adsorption mechanism can be explained by the electrostatic interactions between the negatively charged dye ion and the positive charged sites on the ZnO nanoparticles surface. AR57 and RR are anionic dyes which contains one sulfonic acid group ($-\text{SO}_3\text{Na}$) at AR57 while ($-\text{SO}_3\text{H}$) at RR. (In aqueous solution the dye dissociates to the hydrogen ions (H^+) and the sulfonate anion ($-\text{SO}_3^-$) for RR while for AR57 dissociates to the hydrogen ions (Na^+) and the sulfonate anion ($-\text{SO}_3^-$). At acidic pH, the sulfonic groups can be protonated to the neutral form ($-\text{SO}_3\text{H}$) however, sulfonic groups exhibit negative charge even at higher acidic solutions, due to their pK_a values lower than zero. The mechanism study shows that the existence of Zn^{2+} exposed on the surface of ZnO nanoparticles plays an important role in high adsorption of both AR57 and RR and the ionic bonding between Zn^{2+} and ($-\text{SO}_3^-$). Thus, when the pH of the dye solution decreases, the number of negatively charged sites on FIF decreases and the number of positively charged sites increases which favor the adsorption of negatively charged dye ions because of the electrostatic force of attraction. Therefore, the adsorption capacity of AR57 and RR onto ZnO surface is more favorable at lower pH.

3.3. Thermodynamic parameters

Experiments were carried out at pH 2 and 1.22×10^{-3} M concentration for AR57, and at pH 3 and 1.06×10^{-3} M concentration for RR, adsorbent dosage of 0.02 g in the temperature range of 20–45 °C. The adsorption capacity increased with increases the temperature. This means that this process was endothermic. This could be ascribed to strong of adsorption forces between the active sites of the adsorbent and adsorbate [34].

It is important to investigate the effect of temperature on adsorption in a view of practical application. The adsorption experiments were carried out at pH 2 and 1.22×10^{-3} M concentration for AR57, and at pH 3 and 1.06×10^{-3} M concentration for RR, adsorbent dosage of 0.02 g in the temperature range of 20–45 °C. The adsorption capacity slightly increases from 1.06 to 1.22 mmol g^{-1} for AR57 and from 1.29 to 1.3 mmol g^{-1} for RR with the increase in the temperature from 20 to 45 °C. This behavior confirms that the adsorption process of AR57 and RR onto ZnO nanoparticles is endothermic. This observation can be attributed to

increasing of the mobility of the dye molecules and rate of diffusion of adsorbate molecules across the surface of adsorbent with increasing temperature, which leads to an increase in the adsorption capacity.

The pseudo-second-order rate constant of tested dye adsorption [45] is expressed as a function of temperature by the following Arrhenius type relationship Eq. (10):

$$\ln k_2 = \ln A - E_a/RT \quad (10)$$

The adsorption equilibrium constant, K_c was determined Eq. (11) and used with the Van't Hoff equation (Eq. (12)) and conventional thermodynamic equation (Eq. (13)) for evaluating the thermodynamic constants of the sorbents (i.e., the standard enthalpy change, ΔH° , the standard free Gibbs energy, ΔG° , and the standard entropy change, ΔS°).

$$K_c = \frac{q_e}{C_e} \quad (11)$$

where q_e and C_e are equilibrium concentrations of AR57 and RR on the adsorbent and in the solution, respectively.

$$\Delta G^\circ = -RT \ln K_c \quad (12)$$

$$\Delta G^\circ = \Delta H^\circ - T\Delta S^\circ \quad (13)$$

Therefore the Van't Hoff equation (Eq. (14)) becomes:

$$\ln K_c = \frac{-\Delta H^\circ}{RT} + \frac{\Delta S^\circ}{R} \quad (14)$$

The value of standard enthalpy change (ΔH°) and standard entropy change (ΔS°) for the adsorption process are thus determined from the slope and intercept of the plot of $\ln K_c$ vs. $1/T$. (Figs. 19 and 20). The values of thermodynamic parameters are reported in Table 7. The positive value of ΔH° confirms the endothermic nature of adsorption process. The negative values of ΔG° indicate that the

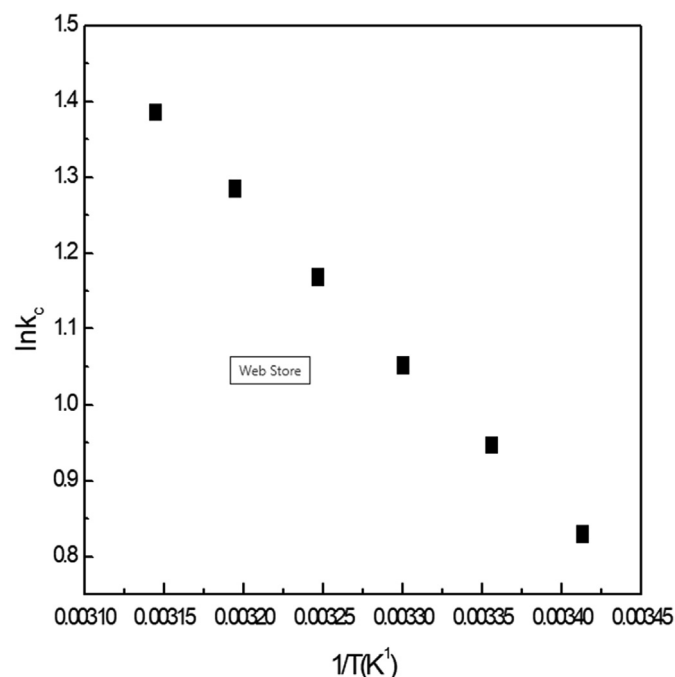


Fig. 19. Van't Hoff plots for AR57 adsorption onto the ZnO nanoparticles at (450 °C) adsorbent.

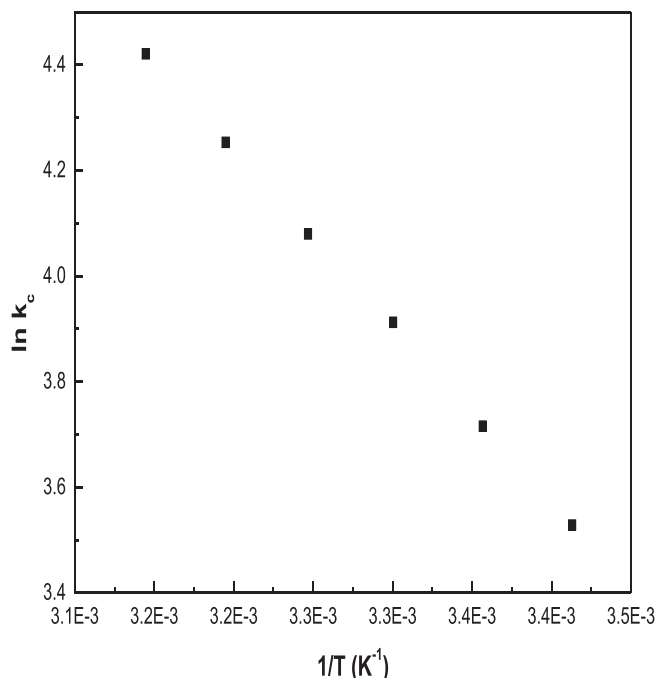


Fig. 20. Van't Hoff plots for RR adsorption onto the ZnO nanoparticles at (450 °C) adsorbent.

adsorption reaction is spontaneous. The increase in the negativity of ΔG° with increasing temperature confirms that the "favorability" increases with temperature [46,47].

3.4. Effect of ionic strength (addition of NaCl)

The effect of chloride ions on Acid Red 57 and Remazol Red removal was examined, by addition of increasing concentrations of NaCl (from 10 to 40 g L⁻¹; C₀: 1.22 × 10⁻³ M; sorbent dosage: 0.02 g, 25 mL) for AR57 while for RR (C₀: 1.06 × 10⁻³ M; sorbent dosage: 0.02 g, 25 mL). For the studied adsorbents increasing the amount of NaCl slightly decreases the sorption capacity: the sorption capacity decreases by about 20%, when NaCl concentration reaches 20 g L⁻¹. This is probably due to the competitor effect of chloride anions against AR57 and RR anions for interaction with the sorption sites [48]. It is noteworthy, that when even NaCl concentration reaches 40 g L⁻¹ the reduction in the adsorption capacity decreases by 1.5%, this indicates that even under these drastic conditions a high adsorption capacity is maintained Figs. 21 and 22.

3.5. Desorption studies

The regeneration ability and stability of the adsorbent are two significant factors influencing the practical application of the adsorbent. We have now compared the adsorption capacity of ZnO for three-consecutive adsorption-desorption cycles. The investigated sorbent ZnO was washed with ethanol several times till colorless and then with distilled water. The colorless product of ZnO was dried at 60 °C for 24 h to a constant weight. After regeneration the adsorbent ready for the second run of uptake [49]. The regeneration efficiency for each adsorption/desorption cycle was found to be 97.6, 92.5, 68.6% and 98.7, 94.2, 66.4% for AR57 and RR, respectively. This can be due to blocking of adsorption sites of ZnO. We have also characterized by XRD of the ZnO material after three cycle test and found that the crystallinity and structure remain intact (Fig. 23). This result shows that the ZnO nanoparticles are

Table 7
Standard enthalpy, entropy and free energy changes for AR57 and RR adsorption on ZnO nanoparticles.

Dye	ΔH° (kJ mol ⁻¹)	ΔS° (J mol ⁻¹ K ⁻¹)	T_0 (K)	ΔG° (kJ mol ⁻¹)				
				293	298	303	308	318
AR57	17.30	65.92	262.49	-2.01	-2.34	-2.67	-2.99	-3.65
RR	27.599	123.55	223.39	-8.6	-9.22	-9.84	-10.45	-11.1

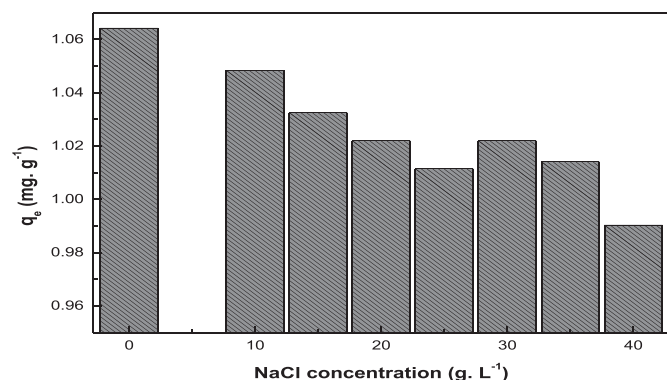


Fig. 21. Influence of NaCl on AR57 adsorption onto the ZnO nanoparticles at 450 °C adsorbent. (C_0 : 1.2×10^{-3} M; initial pH 2; T: 25 °C; sorbent dosage: 0.02 g, 25 mL).

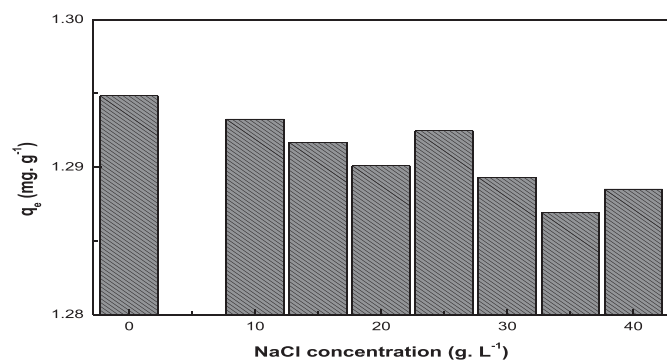


Fig. 22. Influence of NaCl on RR adsorption onto the ZnO at 450 °C adsorbent. (C_0 : 1×10^{-3} M; initial pH 3; T: 25 °C; sorbent dosage: 0.02 g, 25 mL).

having good reusability characteristic [50].

The efficiency of regeneration was calculated using the following equation:

$$\text{Regeneration efficiency (\%)} = \frac{\text{Total adsorption capacity in the second run}}{\text{Total adsorption capacity in the first run}} \times 100 \quad (15)$$

4. Conclusions

The adsorption activity of ZnO nanoparticles was examined for dye solutions such as AR57 and RR. ZnO sample was synthesized by calcination of ZIF-8 at different temperature 450, 550 and 650 °C. The calcination temperature effect on the particle size of synthesized ZnO nanoparticles were characterized by different techniques, for example FTIR, XRD, SEM and EDX measurements. The adsorption of AR57 and RR were systematically investigated under various conditions. The adsorption of these anionic dyes was found

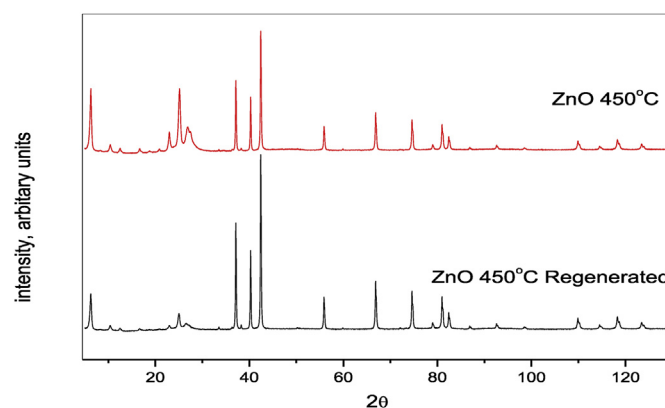


Fig. 23. X-ray diffraction spectra of ZnO nanoparticles at 450 °C and regenerated ZnO.

to be strongly dependent on pH, temperature and contact time. Maximum removal could be achieved at pH 2 and 3 for AR57 and RR, respectively. The adsorption of these dyes was endothermic as the dye removal capacity increase with increase the temperature due to increase of mobility of dye molecules. The Langmuir isotherm model was found to be most suitable model for describing the isotherm for adsorption of both AR57 and RR dyes on ZnO sorbent. In addition, the q_m calculated from Langmuir isotherm was close to the experimental q_{max} . The pseudo-second-order kinetic model agrees very well with the dynamic behavior for the adsorption of AR57 and RR onto ZnO. Also study the effect of temperature and calculation the free Gibbs energy ΔG° it have negative values as the reaction of adsorption for both dyes was endothermic reaction as the adsorption increase with increase of temperature, also study the effect of ionic strength on adsorption process.

Declaration of competing interest

The authors declare that they have no known competing financial interests or personal relationships that could have appeared to influence the work reported in this paper.

CRediT authorship contribution statement

N. Hassan: Conceptualization, Investigation, Writing - original draft, Writing - review & editing, Supervision. **A. Shahat:** Conceptualization, Investigation, Writing - review & editing, Supervision. **A. El-Didamony:** Conceptualization, Investigation, Writing - review & editing, Supervision. **M.G. El-Desouky:** Conceptualization, Investigation, Writing - original draft. **A.A. El-Bindary:** Conceptualization, Investigation, Writing - review & editing, Supervision.

Appendix A. Supplementary data

Supplementary data to this article can be found online at <https://doi.org/10.1016/j.molstruc.2020.128029>.

References

- [1] H. Zhang, Y. Tang, X. Liu, Z. Ke, X. Su, D. Cai, X. Wang, Y. Liu, Q. Huang, Z. Yu, Improved adsorptive capacity of pine wood decayed by fungi *Poria cocos* for removal of malachite green from aqueous solutions, *Desalination* 274 (2011) 97–104.
- [2] P.C.C. Faria, J.J.M. Orfao, M.F.R. Pereira, Adsorption of anionic and cationic dyes on activated carbons with different surface chemistries, *Water Res.* 38 (2014) 2043–2052.
- [3] V.K. Gupta, Suhas, Application of low-cost adsorbents for dye removal—a review, *J. Environ. Manag.* 90 (2009) 2313–2342.
- [4] M.A. Farajzadeh, M.R. Fallahi, Study of phenolic compounds removal from aqueous solution by polymeric sorbent, *J. Chem. Soc.* 52 (2005) 295–301.
- [5] T.H. Kim, C. Park, J. Yang, S. Kim, Comparison of disperse and reactive dye removals by chemical coagulation and fenton oxidation, *J. Hazard Mater.* 112 (2004) 95–103.
- [6] S. Song, J. Fan, Z. He, L. Zhan, Z. Liu, J. Chen, X. Xu, Electrochemical degradation of azo dye CI Reactive Red 195 by anodic oxidation on Ti/SnO₂-Sb/PbO₂ electrodes, *Electrochim. Acta* 55 (2010) 3606–3613.
- [7] B. Shi, G. Li, D. Wang, C. Feng, Removal of direct dyes by coagulation: the performance of preformed polymeric aluminum species, *J. Hazard Mater.* 143 (2007) 567–574.
- [8] G.M. Nisola, E. Cho, A.B. Beltran, M. Han, Y. Kim, W.J. Chung, Dye/water separation through supported liquid membrane extraction, *Chemosphere* 80 (8) (2010) 894–900.
- [9] F. Xia, E. Ou, L. Wang, Photocatalytic degradation of dyes over cobalt doped mesoporous SBA-15 under sunlight, *Dyes Pigments* 76 (2008) 76–81.
- [10] H. Selcuk, Decolorization and detoxification of textile wastewater by ozonation and coagulation processes, *Dyes Pigments* 64 (2005) 217–222.
- [11] C. Theivarasu, S. Mylsamy, N. Sivakumar, Removal of malachite green from aqueous solution by activated carbon developed from cocoa (*Theobroma cacao*) shell: kinetic and equilibrium studies, *Orient. J. Chem.* 27 (2011) 1083–1091.
- [12] F.A. Pavan, S.L.P. Dias, E.C. Lima, E.V. Benvenuto, Removal of Congo red from aqueous solution by anilinepropylsilica xerogel, *Dyes Pigments* 76 (2008) 64–69.
- [13] W. Muhammad, N. Ullah, M. Haroon, B.H. Abbasi, Optical, morphological and biological analysis of zinc oxide nanoparticles (ZnO NPs) using *Papaver somniferum* L, *RSC Adv.* 9 (2019) 29541–29548.
- [14] Y. Feng, Y. Li, M. Xu, S. Liu, J. Yao, Fast adsorption of methyl blue on zeolitic imidazolate framework-8 and its adsorption mechanism, *RSC Adv.* 6 (2016) 109608–109612.
- [15] R. Shirley, *The CRYSFIRE System for Automatic Powder Indexing: User's Manual*, The Lattice Press, England, 2002, 41 Guildford Park Avenue, Guildford, Surrey GU2 7NL.
- [16] H.A. Kiwan, T.M. Atwee, E.A. Azab, A.A. El-Binadary, Efficient photocatalytic deprecation of acid red 57 using synthesized ZnO nanowires, *J. Chin. Chem. Soc.* 66 (2019) 89–98.
- [17] K. Omri, I. Najeh, R. Dhahri, J. El Ghoul, L. El Mir, Effects of temperature on the optical and electrical properties of ZnO nanoparticles synthesized by sol–gel method, *Microelectron. Eng.* 128 (2014) 53–58.
- [18] R. Krithiga, G. Chandrasekaran, Synthesis, structural and optical properties of vanadium doped zinc oxide nanograins, *J. Cryst. Growth* 21 (2009) 311–4610.
- [19] A.L. Patterson, The Scherrer formula for X-Ray particle size determination, *Phys. Rev.* 10 (1939) 56–978.
- [20] O. Mekasuwandumrong, P. Pawinrat, P. Praserttham, J. Panpranot, Effects of synthesis conditions and annealing post-treatment on the photocatalytic activities of ZnO nanoparticles in the degradation of methylene blue dye, *J. Chem. Eng.* 1 (2010) 77–84.
- [21] K. Omri, I. Najeh, L. El Mir, Influence of annealing temperature on the microstructure and dielectric properties of ZnO nanoparticles, *Ceram. Int.* 7 (2016) 8940–8948.
- [22] K. Iman, M. Shahid, M.S. Khan, M. Ahmad, F. Samac, Topology, Magnetism and Dye Adsorption Properties of Metal Organic Frameworks (MOFs) Synthesized from Bench Chemicals, vol. 21, 2019, pp. 5299–5309.
- [23] G. Xiong, U. Pal, J.G. Serrano, K.B. Ucer, R.T. Williams, Photoluminescence and FTIR study of ZnO nanoparticles: the impurity and defect perspective, *Phys. Status Solidi* 3 (2006) 3577–3581.
- [24] D.E. Wurster, E. Oh, J.C. Wang, S. Majuru, Use of Fourier transform infrared (FTIR) spectroscopy to follow the adsorption of heptane and 1,4-dioxane vapors on a zinc oxide surface, *J. Pharmacol. Sci.* 7 (1998) 9–1124.
- [25] M.R. Khanlary, V. Vahedi, A. Reyhani, Synthesis and characterization of ZnO nanowires by thermal oxidation of Zn thin films at various temperatures, *Molecules* 17 (2012) 5021–5029.
- [26] A. Sedky, T.A. El-Brollosy, S.B. Mohamed, Correlation between sintering temperature and properties of ZnO ceramic varistors, *J. Phys. Chem. Solid.* 73 (2012) 505–510.
- [27] A.S. Ozcan, B. Erdem, A. Ozcan, Adsorption of Acid Blue 193 from aqueous solutions onto Na–bentonite and DTMA–bentonite, *J. Colloid Interface Sci.* 280 (1) (2004) 44–54.
- [28] Z. Wu, I.-S. Ahn, C.-H. Lee, J.-H. Kim, Y.G. Shul, K. Lee, Enhancing the organic dye adsorption on porous xerogels, *Colloids Surf., A* 240 (1–3) (2004) 157–164.
- [29] I. Kiran, T. Akar, A.S. Ozcan, A. Ozcan, S. Tunali, Biosorption kinetics and isotherm studies of acid red 57 by dried cephalosporium aphidicola cells from aqueous solutions, *Biochem. Eng. J.* 31 (2006) 197–203.
- [30] M. Yavuz, F. Gode, E. Pehlivan, S. Ozmert, Y.C. Sharma, An economic removal of Cu²⁺ and Cr³⁺ on the new adsorbents: pumice and polyacrylonitrile/pumice composite, *Chem. Eng. J.* 137 (2008) 453–461.
- [31] K.Z. Elwakeel, A.A. El-Bindary, E.Y. Kouta, E. Guibal, Functionalization of polyacrylonitrile/Na–Y-zeolite composite with amidoxime groups for the sorption of Cu(II), Cd(II) and Pb(II) metal ions, *Chem. Eng. J.* 332 (2018) 727–736.
- [32] S. Wong, N.A.N. Yac'cob, N. Ngadi, O. Hassan, I.M. Inuwa, From pollutant to solution of wastewater pollution: synthesis of activated carbon from textile sludge for dye adsorption, *J. Chem. Eng.* 26 (2018) 870–878.
- [33] W.A. Khanday, F. Marrakchi, M. Asif, B.H. Hameed, Mesoporous zeolite-activated carbon composite from oil palm ash as an effective adsorbent for methylene blue, *J. Taiwan Inst. Chem. Eng.* 70 (2017) 32–41.
- [34] N. Sharma, B.K. Nandi, Utilization of sugarcane bagasse, an agricultural waste to remove malachite green dye from aqueous solutions, *J. Mater. Environ. Sci.* 4 (2013) 1052–1065.
- [35] I. Langmuir, The constitution and fundamental properties of solids and liquids. II. Liquids, *J. Am. Chem. Soc.* 39 (1917) 1848–1906.
- [36] I. Langmuir, The adsorption of gases on plane surfaces of glass, mica and platinum, *J. Am. Chem. Soc.* 40 (1918) 1361–1403.
- [37] H. Freundlich, W. Heller, The adsorption of *cis*- and *trans*-azobenzene, *J. Am. Chem. Soc.* 61 (1939) 2228–2230.
- [38] M.M. Dubinin, E.D. Zaverina, L.V. Radushkevich, Sorption and structure of active carbons. I. Adsorption of organic vapors, *Zh. Fiz. Khim.* 21 (1947) 1351–1362.
- [39] M.J. Temkin, V. Pyzhev, Recent modifications to Langmuir isotherms, *Acta Physicochim. URSS* 12 (1940) 217–222.
- [40] S. Lagergren, Zur theorie der sogenannten adsorption gelöster stoffe, *Kungliga Svenska Vetenskapsakad. Handl* 24 (1898) 1–39.
- [41] Y.S. Ho, G. McKay, Sorption of dye from aqueous solution by peat, *Chem. Eng. J.* 70 (2) (1998) 115–124.
- [42] J. Zeldowitsch, Über den Mechanismus der katalytischen Oxydation von CO und MnO₂, *Acta Physicochim. URSS* 1 (1934) 364–449.
- [43] M.H. Dehghani, A. Dehghan, A. Najafpoor, Removing reactive red 120 and 196 using chitosan/zeolite composite from aqueous solutions: kinetics, isotherms, and process optimization, *J. Ind. Eng. Chem.* 51 (2017) 185–195.
- [44] Y. Zhang, G. Huang, C. An, X. Xin, X. Liu, M. Raman, Y. Yao, W. Wang, M. Doble, Transport of anionic azo dyes from aqueous solution to gemini surfactant-modified wheat bran: synchrotron infrared, molecular interaction and adsorption studies, *Sci. Total Environ.* 595 (2017) 723–732.
- [45] M.M.R. Khan, M. Ray, A.K. Guha, Mechanistic studies on the binding of Acid Yellow 99 on coir pith, *Bioresour. Technol.* 102 (2011) 2394–2399.
- [46] H. Nollet, M. Roels, P. Lutgen, P. Van der Meer, W. Verstraete, Removal of PCBs from wastewater using fly ash, *Chemosphere* 53 (6) (2003) 655–665.
- [47] M.R. Fathi, A. Asfaram, A. Farhangi, Removal of direct red 23 from aqueous solution using corn stalks: isotherms, kinetics and thermodynamic studies, *Spectrochim. Acta A* 135 (2015) 364–372.
- [48] C. Prasad, S. Karlapudi, P. Venkateswarlu, I. Bahadur, S. Kumar, Green arbitrated synthesis of Fe₃O₄ magnetic nanoparticles with nanorod structure from pomegranate leaves and Congo red dye degradation studies for water treatment, *J. Mol. Liq.* 240 (2017) 322–328.
- [49] J. Liu, H. Yu, Q. Liang, Y. Liu, J. Shen, Q. Bai, Preparation of polyhedral oligomeric silsesquioxane based cross-linked inorganic-organic nanohybrid as adsorbent for selective removal of acidic dyes from aqueous solution, *J. Colloid Interface Sci.* 497 (2017) 402–412.
- [50] A.A. El-Bindary, S.M. El-Marsafy, A.A. El-Maddah, Enhancement of the photocatalytic activity of ZnO nanoparticles by silver doping for the degradation of AY99 contaminants, *J. Mol. Struct.* 1191 (2019) 76–84.